Journal of Alloys and Compounds 503 (2010) L1–L4

Contents lists available at ScienceDirect

Journal of Alloys and Compounds

journal homepage: www.elsevier.com/locate/jallcom

Letter

Ni@Pt core–shell nanoparticles with enhanced catalytic activity for oxygen reduction reaction

Guoxiu Wang[a,c,*], Huimin Wu[a], David Wexler[a], Huakun Liu[a], Oumarou Savadogo[b]

[a] Institute for Superconducting and Electronic Materials, School of Mechanical, Materials and Mechatronics Engineering, University of Wollongong, NSW 2522, Australia
[b] Materials Engineering Department, Ecole Polytechique de Montréal, Montreal, Qc, H3C3A7, Canada
[c] Department of Chemistry and Forensic Science, University of Technology Sydney, Sydney, NSW 2007, Australia

ARTICLE INFO

Article history:
Received 12 February 2010
Received in revised form 8 April 2010
Accepted 21 April 2010
Available online 6 May 2010

Keywords:
Core–shell nanostructure
Oxygen reduction reaction
Ni@Pt nanoparticles
PEM fuel cell

ABSTRACT

Ni@Pt core–shell nanoparticles were synthesized by chemical reduction and sequential chemical deposition. The as-prepared nanoparticles were characterized by X-ray diffraction and high resolution transmission electron microscopy. Cyclic voltammetry and steady-state polarization measurements revealed that the Ni@Pt core–shell nanoparticles have much higher catalytic activity towards oxygen reduction than that of commercial BASF 20 wt Pt% catalyst. Ni@Pt core–shell nanoparticles only contain 16.7 at Pt%, therefore having a significantly reduced cost. Core–shell nanostructures could be a promising strategy to reduce the catalyst costs, but still maintain high catalytic reactivity.

1. Introduction

Hydrogen fed polymer electrolyte membrane fuel cells (PEMFCs) provide zero-emission power sources for automobiles and distributed power generation [1,2]. The major challenge for widespread applications of PEMFCs relates to the performance, durability, and cost of anode and cathode catalysts [3,4]. Platinum (Pt) nanoparticles have been mainly used as catalysts both for the hydrogen oxidation reaction (HOR) and the oxygen reduction reaction (ORR). In order to reduce the cost and to improve the catalytic activity of catalyst materials, many efforts have been devoted to developing Pt-transition metal alloy catalysts. For examples, Pt–Co, Pt–Ni, Pt–Fe, Pt–Cu, Pt–Ru, Pt–Sn, and Pt–Mo alloy nanoparticles have been chemically synthesized and electrochemically tested [5–11]. These bimetallic alloy catalysts have shown promise for reducing the loading of Pt, but still maintaining high catalytic activity.

A variety of core–shell nanoparticles have also been reported as catalysts in PEMFCs. Dealloyed Pt–Cu core–shell nanoparticles were prepared by selective dissolution of Cu atoms from nanoparticle surfaces and have demonstrated surface catalytic improvement towards oxygen reduction [12,13]. It was proposed that a reduced Pt–Pt distance near the particle surface stabilized by the lattice contracted alloy core might be responsible for the surface catalytic reactivity. Ru–Pt core–shell nanoparticles showed preferential oxidation of carbon monoxide in hydrogen and remarkable improvement of catalytic reactivity. Density functional theory studies suggested that the enhanced catalytic activity for the core–shell nanoparticle originates from a combination of an increased availability of CO-free Pt surface sites on the Ru@Pt nanoparticles and a hydrogen-mediated low-temperature CO oxidation process that is clearly distinct from the traditional bifunctional CO oxidation mechanism [14]. Polymer protected Pd@Pt core–shell nanostructures were synthesized by a hydrogen-sacrificial strategy. The better catalytic performance of core–shell nanoparticles could be related to near surface alloy (NSA) effects, in which subsurface metal and alloys layers affect the binding of adsorbates to the particle surface. The changes in binding enthalpies can enhance rates and selectivity in the catalytic process [15,16]. Therefore, the core–shell structure is an ideal nano-architecture for reducing the cost of catalyst material and improving catalytic reactivity.

A number of synthesis strategies have already been used for the production of core–shell structure catalysts, such as redox-transmetalation [17], ethylene glycol-assisted polyol method [18], co-reduction [19], seed growth method [20], etc. Herein, we report the synthesis, characterization, and electrochemical performance of novel Ni@Pt core–shell nanoparticles as catalyst for oxygen reduction reaction.

2. Experiment

All chemicals were ACS Reagent and purchased from Sigma–Aldrich. In a typical synthesis process, 0.357 mol/L potassium hydroxide, 0.0242 mol/L oleylamine, 0.007 mol/L nickel acetate tetrahydrate in 130 ml 1,2-propanediol solution were

* Corresponding author. Tel.: +61 2 42215726; fax: +61 2 42215731.
E-mail address: Guoxiu.Wang@uts.edu.au (G. Wang).

0925-8388/$ – see front matter © 2010 Elsevier B.V. All rights reserved.
doi:10.1016/j.jallcom.2010.04.236

heated to 120 °C in a three-neck round-bottom flask under flowing argon gas. After stirring for 30 min, the green mixture was further heated to 135 °C, to which a solution of 1.125 mol/L sodium boronhydride in 8 ml hydrazine hydride was gradually added under an argon atmosphere. The solution turned black, indicating the reduction of Ni^{2+} to Ni nanoparticles. Then, a fixed amount of chloroplantinic acid hexahydrate was added to the mixture to obtain Ni@Pt core–shell nanoparticles with a nominal atomic ratio of Pt:Ni = 1:5. Finally, the resulting dispersion was left to cool down to room temperature and then separated by centrifugation. The as-synthesised Ni@Pt nanoparticles were characterised by X-ray diffraction (XRD; GBC MMA X-ray diffractometer with Cu Kα radiation) and transmission electron microscopy (TEM; JEOL JEM 2011 TEM facility).

Ni@Pt/C electrocatalysts were prepared by dispersing Ni@Pt nanoparticles on Vulcan XC-72 carbon according to the weight ratio of Ni@Pt:C = 20:80, and the mixture was stirred overnight. Then, the electrode ink was prepared by adding 5 mg Ni@Pt/C catalyst powders to a 5 wt% Nafion solution (Dupont™, 1 ml). The ink was then ultrasonicated for 1 h. The catalyst ink was then painted onto a glassy carbon (GC) electrode by using a microsyringe and thermally treated for 1 h at 60 °C for 1 h. Electrochemical measurements were performed using a glassy carbon rotating disk electrode (ROE, model AFMSRCE, Pine Research Instrumentation) connected to a bipotentiostat (AFCBPIE, Pine Research Instrumentation). The counter electrode was a Pt wire, and the reference electrode was a saturated calomel electrode (SCE). The electrolyte solution was 0.5 M H_2SO_4 solution. As a comparison, the electrochemical performance of the commercial Pt/C catalyst BASF (20% Pt supported on Vulcan XC-72 carbon, BASF Chemical) was also examined.

3. Results and discussion

Fig. 1a shows the X-ray diffraction pattern of Ni@Pt core–shell nanoparticles. We noticed that only diffraction peaks of Ni phase appeared in the XRD pattern. This could be because that outer Pt layer is too thin and in amorphous status to be visible to X-ray diffraction. All diffraction lines can be indexed to the fcc cubic

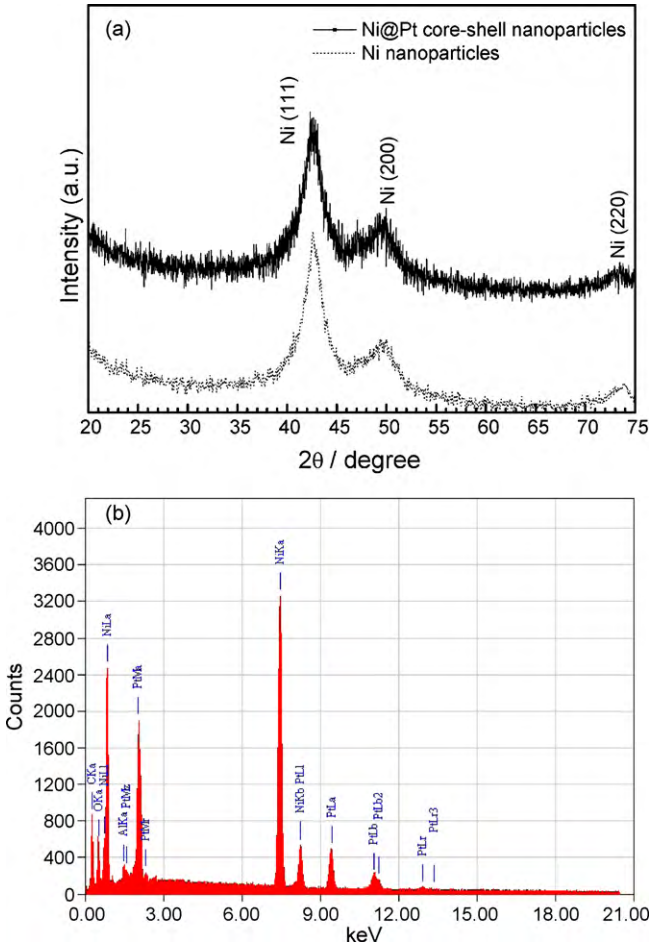

Fig. 1. (a) X-ray diffraction pattern of Ni@Pt core–shell nanoparticles and Ni nanoparticles. (b) EDX spectrum of Ni@Pt core–shell nanoparticles.

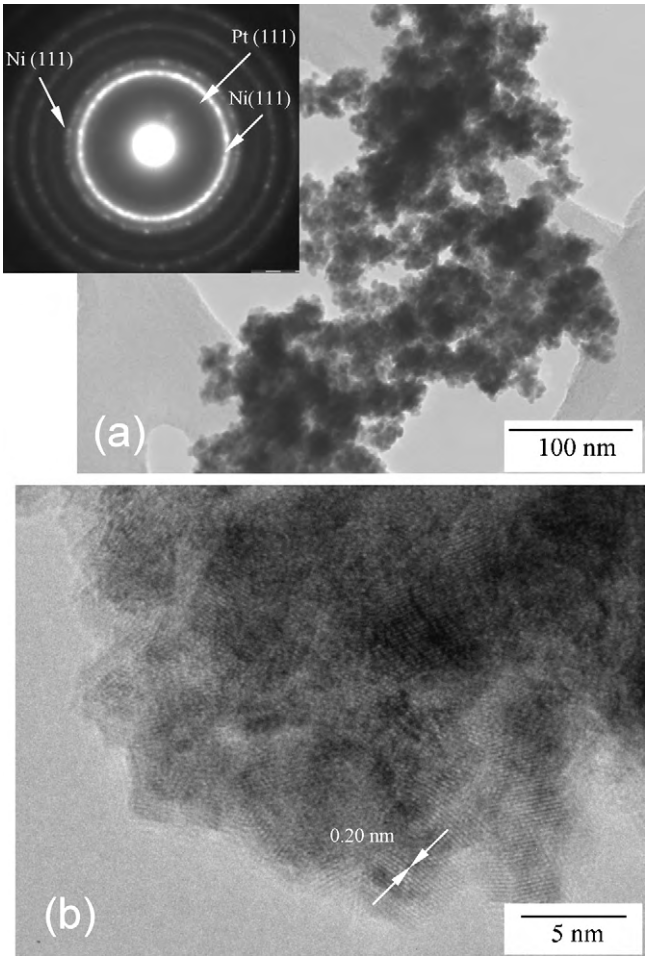

Fig. 2. (a) Low magnification TEM image of Ni@Pt nanoparticles. The inset is the corresponding SAED pattern. (b) Lattice resolved high resolution TEM image of Ni@Pt nanoparticles.

Ni phase with the space group: *Fm*-3*m*, 225. No characteristic diffraction peaks of nickel oxides were detected, indicating that the oxidation of Ni can be effectively prevented by flowing argon gas during the reduction process. As a comparison, the XRD pattern of Ni nanoparticles is also presented in Fig. 1a. Ni@Pt core–shell nanoparticles and Ni nanoparticles show the same X-ray diffraction pattern.

The morphologies of the as-prepared Ni@Pt catalyst nanoparticles were analyzed by field emission scanning electron microscope (FESEM) and TEM observation. We also performed quantitative energy dispersive X-ray analysis (EDX) on the FESEM sample. The atomic ratio of Pt:Ni was determined to be 19.8: 100.4, which is very close to the nominal ratio of 1: 5. The EDX spectrum of Ni@Pt core–shell nanoparticles is shown in Fig. 1b. Fig. 2a shows a low magnification TEM image of Ni@Pt nanoparticles, from which we can see that the nanoparticles tend to stick together to form loose agglomerates. The associated selected area electron diffraction pattern (SAED) is shown as the inset in Fig. 2a. The major diffraction rings can be indexed to be the cubic nickel phase. As labeled on the SAED pattern, one weak diffraction ring can be identified as Pt(1 1 1), which confirms the co-existence of Ni and Pt phase. Fig. 2b shows a lattice resolved high resolution TEM (HRTEM) image of Ni@Pt core–shell nanoparticles. The lattice planes with a interlayer distance of 0.2 nm in the core can be indexed to (1 1 1) crystal planes of Ni. The outer layer of the nanoparticles shows different contrast, which is attributed to be a thin Pt layer deposited on the Ni core to form the core–shell nanostructure.

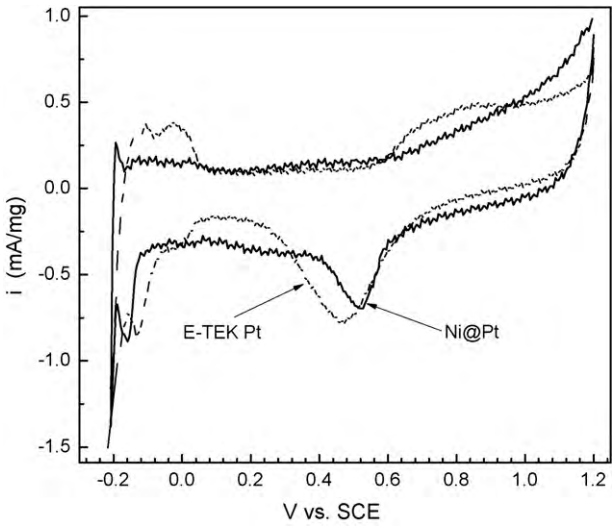

Fig. 3. Cyclic voltammograms of Ni@Pt core–shell nanoparticles and E-TEK 20 wt% Pt catalyst in 0.5 M H_2SO_4 electrolyte. Scanning rate: 50 mV/s.

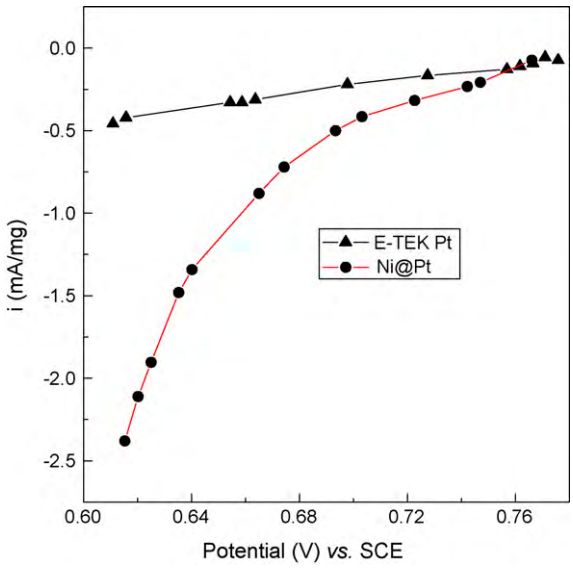

Fig. 4. Linear scan voltammograms for Ni@Pt nanoparticles and E-TEK 20 wt% Pt catalyst in 0.5 M H_2SO_4 solution saturated with oxygen. Rotating the electrode: 1600 rpm, scan rate: 5 mV/s.

The electrocatalytic activities towards ORR of the as-prepared Ni@Pt nanoparticles and the commercial Pt catalyst were evaluated by cyclic voltammetry (CV). The measurements were performed in a 0.5 M H_2SO_4 aqueous electrolyte. Fig. 3 exhibited two distinctive potential regions associated with H_{upd} adsorption/desorption process ($H^+ + e = H_{upd}$) between $0\,V < E < 0.35\,V$ and the formation of a OH_{ad} layer ($2H_2O = OH_{ad} + H_3O^+ + e$) beyond 0.60 V, where H_{upd} and OH_{ad} refer to the underpotentially deposited hydrogen and the adsorbed hydroxyl species, respectively. Furthermore, the Ni@Pt core–shell nanoparticle catalyst exhibited well defined current peaks associated with hydrogen adsorption–desorption processes on a Pt surface, implying a Pt nature of the particle surface. And the current peak associated with the reduction of hydroxyl species in the CV obtained from the Ni@Pt nanoparticles shifts more than 75 mV toward positive potential as compared to that of a pure Pt nanoparticles. This indicates that the oxygenate species on the surface of the Ni@Pt nanoparticles have weaker adsorption energy than that on the pure Pt catalysts, indicating facilitated desorption of oxygenated Pt species [21–24]. A major decline in the fuel-cell's efficiency was partly attributed to the inhibition of O_2 reduction caused by OH adsorption on Pt in the potential region 0.75–1 V [25,26]. Therefore, the weak adsorption of the hydroxyl species would increase the surface active sites for ORR [22,27–32] and the fuel-cell's efficiency. By measuring the charges collected in the H_{upd} adsorption/desorption region after double-layer correction and assuming a value of 210 $\mu C/cm^2$ for the adsorption of a hydrogen monolayer [33], the specific electrochemically active surface areas (ECSA) of the catalysts were calculated to be 70.2 m^2/g for Ni@Pt core–shell nanoparticles and 80.1 m^2/g for the BASF Pt catalyst, respectively. The lower ECSA value of the Ni@Pt nanoparticles can rule out surface roughening as the origin of the enhanced ORR catalytic activity. Therefore, both surface structure effects and electronic effects could be responsible for the enhanced ORR catalytic activity for Ni@Pt core–shell nanoparticles. As previously reported, the d-band density of states (DOS) of Pt is downshifted to lower energy for the Ni@Pt-skin structure, inducing a correlated change of chemisorption energies [34–36]. On the other hand, the Ni-induced modification of the Pt-skin electronic structure can increase the number of active sities for O_2 adsorption [37,38].

The LSV curves were measured in O_2 saturated solution to investigate the ORR activity of the Ni@Pt catalyst in 0.5 M H_2SO_4. And the activity of commercial Pt/C (BASF) under O_2 atmosphere was also investigated as the comparison. We can calculate the total quantity catalyst used on the electrodes, so we can translate the current (mA) to current (mA/g), which can be more effective to interpret the catalytic activities. As shown in Fig. 4, the currents of the Ni@Pt are higher than that of BASF Pt/C in the potential range. It is attributed that Ni@Pt core–shell catalyst exhibited much higher catalytic activity towards the ORR than that the BASF 20% Pt catalyst, which is in accordance with the positive shift of the ORR peak in the CV curves. Therefore, both cyclic voltammetry and polarization measurements confirmed the enhanced ORR catalytic activity for Ni@Pt core–shell nanoparticles.

4. Conclusion

In summary, Ni@Pt core–shell nanoparticles with an atomic ratio of Ni:Pt = 5:1, were synthesized by sequential chemical reduction under the assistance of surfactants. X-ray diffraction and high resolution TEM analysis confirmed the core–shell nanostructure. The electrochemical performance of Ni@Pt nanoparticles as catalyst for ORR was evaluated by cyclic voltammetry and steady-state polarization. The results show that Ni@Pt nanoparticles exhibited much enhanced catalytic activity towards ORR compared to the commercial E-TEK pure Pt catalyst.

Acknowledgement

We acknowledge financial support from the Australian Research Council (ARC) through an ARC Linkage project, "Exploration of new catalyst materials for hydrogen/air fed proton exchange membrane fuel cells" (LP0775109).

References

[1] D.J. Berger, Science 286 (2999) 49.
[2] G. Brumfiel, Nature 422 (2003) 104.
[3] V. Dusastre, Nature 414 (2001) 331.
[4] R. Bashyam, P. Zelenay, Nature 443 (2006) 63.
[5] L. Xiong, A.M. Kannan, A. Manthiram, Electrochem. Commun. 4 (2002) 898.
[6] L. Xiong, A. Manthiram, Electrochim. Acta 50 (2005) 2323.
[7] H.M. Wu, D. Wexler, G.X. Wang, J. Alloys Compd. 488 (2009) 195.
[8] N.P. Lebedeva, G.J.M. Janseen, Electrochim. Acta 51 (2005) 29.
[9] J.H. Zeng, J.Y. Lee, J. Power Sources 140 (2005) 268.
[10] D. Lee, S.W. Hwang, I. Lee, J. Power Sources 145 (2005) 147.
[11] G. Chen, D.G. Xia, Z.R. Nie, Z.Y. Wang, L. Wang, J.J. Zhang, Chem. Mater. 19 (2007) 1840.

[12] S.H. Zhou, B. Varughese, B. Eichhorn, G. Jackson, K. McIlwrath, Angew. Chem. Int. Ed. 44 (2005) 4539.
[13] P. Mani, R. Srivastava, P. Strasser, J. Phys. Chem. C 112 (2008) 2770.
[14] A. Alayoglu, A.U. Nilekar, M. Mavrikakis, B. Eichhorn, Nat. Mater. 7 (2008) 333.
[15] Y. Wang, N. Toshima, J. Phys. Chem. B 101 (1997) 5301.
[16] V.R. Stamenkovic, B. Fowler, B.S. Mun, G.F. Wang, P.N. Ross, C.A. Lucas, N.M. Markevic, Science 315 (2007) 493.
[17] D. Chen, J. Li, C. Shi, X. Du, N. Zhao, J. Sheng, S. Liu, Chem. Mater. 19 (2007) 3399.
[18] R. Harpness, A. Gedanken, Langmuir 20 (2004) 3431.
[19] S. Nath, S. Praharaj, S. Panigrahi, S.K. Ghosh, S. Kundu, S. Basu, T. Pal, Langmuir 21 (2005) 10405.
[20] I. Srnova-Sloufova, B. Viekova, Z. Bastl, T. Hasslet, Langmuir 20 (2004) 3407.
[21] K. Hiroshima, T. Asaoka, T. Noritale, Y. Ohya, Y. Morimoto, Fuel Cells 2 (2002) 31.
[22] M.H. Shao, K. Sasaki, R.R. Adzic, J. Am. Chem. Soc. 128 (2006) 3526.
[23] J.K. Norskov, J. Rossmeisl, A. Logadottir, L. Lindqvist, J.R. Kitchin, T. Bligaard, H. Jonsson, J. Phys. Chem. B 108 (2004) 17886.
[24] V. Stamenkovic, B.S. Moon, K.J. Mayerhofer, P.N. Ross, C.A. Lucas, N. Markovic, J. Rossmeisl, J. Greely, J.K. Norskov, Angew. Chem. Int. Ed. 45 (2006) 2897.
[25] V. Stamenkovic, B.S. Moon, M. Arenz, K.J. Mayerhofer, C.A. Lucas, G. Wang, P.N. Ross, N. Markovic, Nat. Mater. 6 (2007) 241.
[26] J.X. Wang, N.M. Markovic, R.R. Adzic, J. Phys. Chem. B 108 (2004) 4127.
[27] N.M. Markovic, T.J. Schmidt, V. Stamenkovic, P.N. Ross, Fuel Cells 1 (2001) 105.
[28] V.R. Stamenkovic, B. Fowler, B.S. Mun, G.F. Wang, P.N. Ross, C.A. Lucas, N.M. Markovic, Science 315 (2007) 493.
[29] V. Stamenkovic, T.J. Schmidt, P.N. Ross, N.M. Markovic, J. Phys. Chem. B 106 (2002) 11970.
[30] V. Stamenkovic, T.J. Schmidt, P.N. Ross, N.M. Markovic, J. Electroanal. Chem. 191 (2003) 554.
[31] V.R. Stamenkovic, B.S. Mun, K.J.J. Mayrhofer, P.N. Ross, N.M. Markovic, J. Am. Chem. Soc. 128 (2006) 8813.
[32] S. Mukerjee, S. Srinivasan, M.P. Soriaga, J. McBreen, J. Electrochem. Soc. 142 (1995) 1409.
[33] T.J. Schmidt, et al., J. Electrochem. Soc. 145 (1998) 2354.
[34] B. Hammer, J.K. Norskov, Adv. Catal. 45 (2000) 71.
[35] B. Lim, M. Jiang, P.H.C. Camargo, E.C. Cho, J. Tao, X.M. Lu, Y.M. Zhu, Y.N. Xia, Science 324 (2009) 1302.
[36] J. Greeley, J.K. Norskov, Surf. Sci. 592 (2005) 104.
[37] P. Strasser, Q. Fan, M. Devenney, W.H. Weunberg, P. Liu, J.K. Norskov, J. Phys. Chem. B 107 (2003) 11013.
[38] V. Stamenkovic, B. Fowler, B.S. Moon, G.F. Wang, P.N. Ross, C.A. Lucas, N.M. Markovic, Science 315 (2007) 493.